TWO-PENDULUM MODEL OF PROPELLANT SLOSH IN EUROPA CLIPPER PMD TANK

Wanyi Ng and David Benson
NASA GSFC 597, Civil Servants, Authors

ABSTRACT

The objective of this fluids analysis is to model propellant slosh for the Europa Clipper mission using a two-pendulum model, such that controls engineers can predict slosh behavior during the mission. Propellant slosh causes shifts in center of mass and exerts forces and torques on the spacecraft which, if not adequately controlled, can lead to mission failure. The two-pendulum model provides a computationally simple model that can be used to predict slosh for the Europa Clipper tank geometry. The Europa Clipper tank is cylindrical with a domed top and bottom and includes a propellant management device (PMD). Due to the lack of experimental data in low gravity environments, computational fluid dynamics (CFD) simulation results were used as "real" slosh behavior for two propellants at three fill fractions. Key pendulum parameters were derived that allow the pendulum model's center of mass, forces, and moments to closely match the CFD data. The parameter trends were examined as a function of tank fill fraction and compared with solutions to analytic equations that describe the frequency of slosh in tanks with simple geometries. The trends were monotonic as expected, and parameters resembled analytical predictions; any differences could be explained by the specific differences in the geometry of the tank. This paper summarizes the new method developed at Goddard Space Flight Center (GSFC) for deriving pendulum parameters for two-pendulum equivalent sloshing models. It presents the results of this method and discusses the validity of the results. This analysis is at a completed stage and will be applied in the immediate future to the evolving tank geometry as Europa Clipper moves past its preliminary design review (PDR) phase.

INTRODUCTION

When liquid propellant sloshes in a tank, it shifts the center of mass (CM) of spacecraft and exerts forces and torques on the spacecraft. This motion must be predicted and accounted for in the spacecraft design to achieve mission success. In the past, NASA's Solar Dynamics Observatory (SDO) was forced to enter safe mode when the attitude control system was unable to accurately point the spacecraft due to fuel slosh (Mason, 2011). If slosh motion can be accurately predicted, attitude control systems (ACS) thrusters can be sized to adequately counteract the forces and torques and resonant frequencies of the system can be avoided. The ability to predict slosh behavior is especially important in Europa Clipper because the propellant makes up such a large percentage of the total spacecraft mass. The most accurate means of determining slosh behavior, short of performing experiments in low gravity, is using computational fluid dynamics (CFD). However, these simulations are very computationally

expensive and can take several days to generate a few minutes' worth of data. As a result, pendulum models are used as an approximation of the slosh. A few representative CFD cases are run to calibrate key parameters in the pendulum model, and interpolation can be used to approximate the pendulum parameters between CFD cases. Single-pendulum models are commonly used in slosh modeling, but they are less accurate than two-pendulum models for tanks containing a sponge propellant management device (PMD), like the ones on Europa Clipper. This paper summarizes a new method for determining pendulum parameters for a two-pendulum model. It then presents the results, examines the trends in comparison with existing literature, and discusses of validity of the pendulum models for one iteration of Europa Clipper's propellant tanks.

THEORY

Computational Fluid Dynamics (CFD) Model Setup

The CFD program STAR-CCM+ was used for the Europa slosh analysis. The CFD provided the center of mass, forces, and moment on the tank during the sloshing event. In addition, the CFD program outputted the moment of inertia of the settled propellant. This program has been used successfully in the past by NASA Goddard Space Flight Center to determine slosh for the ICESat-2 and OSIRIS-Rex missions.

CFD simulations were run for each of the two propellants, nitrogen tetroxide (NTO) and monomethyl hydrazine (MMH) at three different tank fill fractions. The propellant properties were calculated from equations provided in the United States Air Force handbooks on hydrazine fuels (Marsh, 1970) and nitrogen tetroxide oxidizers (Wright, 1977).

The liquid surface was initialized at a 15-degree angle from horizontal for all cases unless otherwise noted. This pendulum initial offset angle was assumed to be equal to the fluid surface angle. Figure 1 below shows what an offset of the liquid surface looked like. The PMD vanes are also shown outlined in black.

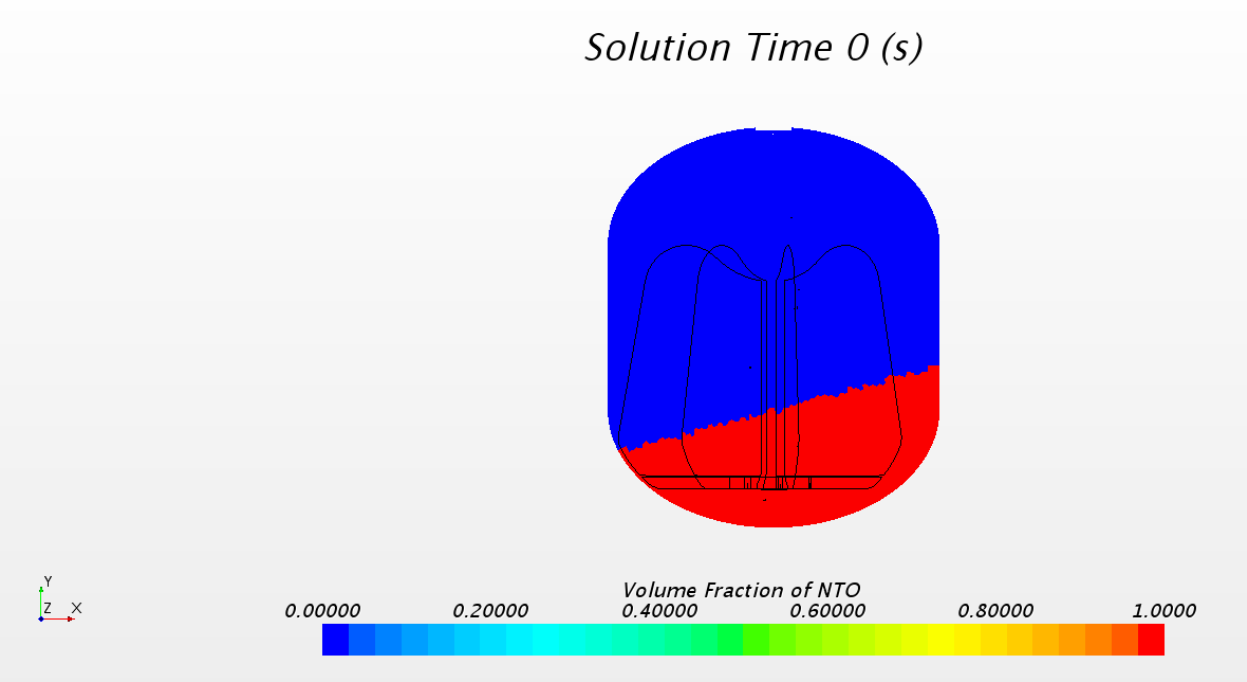

Figure 1. Offset of liquid of 15 deg with no surface tension model turned on at a fill fraction of 35%.

The acceleration was applied in the CFD model using the gravity model.

The volume of the tank was discretized using a polyhedral mesh with growth cells at the solid boundaries (called prism mesh cells in STAR-CCM+). A mesh independence study was done to determine appropriate mesh refinement and parameter selection.

The CFD program output tables for the propellant center of mass location, forces, and torques exerted on the tank in three cartesian coordinates – one along the axis of the tank and two transverse orthogonal directions. The program also outputted the moment of inertia of the liquid and gas as well as images of the volume fractions of liquid and gas.

The models were released from the initial offset and allowed to settle for sufficient time to determine the sloshing frequency and damping.

Pendulum Model Derivation

A damped pendulum's movement can be described by the equations below.

$$I\frac{d^2\theta}{dt^2} = \tau$$

Equation 1

$$ml^2\frac{d^2\theta}{dt^2} + 2\zeta\omega ml^2\frac{d\theta}{dt} + mglsin\theta = 0$$

Equation 2

Equation 1 shows that the moment of inertia of the pendulum, I, multiplied by the angular acceleration, $\frac{d^2\theta}{dt^2}$, is equal to the torque, τ. For a damped pendulum, Equation 1 becomes Equation 2 where m is the mass of the pendulum, l is the length of the pendulum, g is the spacecraft acceleration, ω is the undamped frequency of the pendulum, ζ is the damping ratio, and θ is the angle of the pendulum from the resting position. The forces used to obtain Equation 2 are shown in Figure 2.

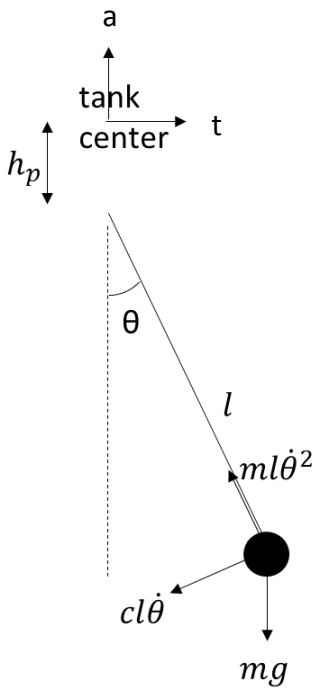

Figure 2. Forces on pendulum bob.

A positive rotation is counter-clockwise. By dividing by ml^2, by noting that ω^2 is equal to $\frac{g}{l}$, and by assuming a small angle approximation, Equation 3 can be obtained.

$$\frac{d^2\theta}{dt^2} + 2\zeta\omega\frac{d\theta}{dt} + \omega^2\theta = 0$$

Equation 3

Equation 3 is an ordinary differential equation and there are known methods for solving it. The result is shown below in Equation 4, with θ_0 being the initial pendulum offset angle.

$$\theta(t) = \theta_0 e^{-\zeta\omega t}\left(\frac{\zeta\omega}{\omega\sqrt{1-\zeta^2}}\sin\left(\omega\sqrt{1-\zeta^2}\,t\right) + \cos\left(\omega\sqrt{1-\zeta^2}\,t\right)\right)$$

Equation 4

Note that Equation 4 predicts no slosh if θ_0 is equal to zero. This is why the CFD simulation requires the surface to be offset to one side.

The unknowns in Equation 4 are ζ, ω, and θ_0. If ω is determined, the length of the pendulum, l, can be calculated using the relation in Equation 5.

$$\omega = \sqrt{\frac{g}{L}}$$

Equation 5

In addition, the hinge location, h_p, the static mass, m_0, and the static mass location, h_0 need to be found to accurately calculate the force in the axial direction and the moments applied to the tank. All quantities are fixed within the model for a given propellant fill fraction, except for the pendulum angle, which is a function of time.

To solve for the unknowns, the pendulum parameters are solved so the pendulum model output fits the CFD model outputs.

The forces that the pendulum exerts on the tank walls are calculated in Equation 6 and Equation 7. Equation 6 is the summation of the forces in the transverse direction due to the pendulum and Equation 7 is used to calculate the summation of the forces in the axial direction due to the pendulum. (Note: Equation 7 can be modified to include the term $-m_0 g$, the inertial force on the static mass, if matching with the forces in the axial direction from the CFD. But this added force will not cause a moment because the static mass stays on the axial line of the tank, and so should not be used in Equation 8). The summation of the moments was found using Equation 8, where g is the spacecraft acceleration, l_a and l_t are the moment arms in the axial and lateral directions, respectively. In this coordinate system, the *z* coordinate is in the direction orthogonal to both *a* and *t*.

$$F_t = ml\left(\frac{d\theta}{dt}\right)^2 \sin(\theta) - ml\frac{d^2\theta}{dt^2}\cos(\theta)$$

Equation 6

$$F_a = -ml\left(\frac{d\theta}{dt}\right)^2 \cos(\theta) - ml\frac{d^2\theta}{dt^2}\sin(\theta) - mg$$

Equation 7

$$M_z = -F_t l_a + F_a l_t$$

Equation 8

Figure 3 illustrates the forces exerted by the pendulum on the tank.

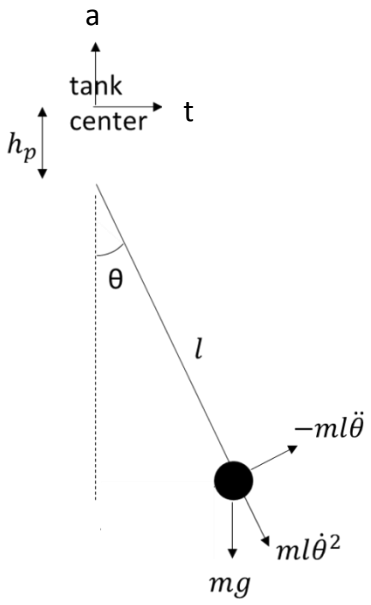

Figure 3. Forces exerted by pendulum on tank.

The parameters *m,* ζ, and ω (components of $\theta(t)$) were selected such that the pendulum motion closely matches the CFD data.

The hinge point, h_p, for each pendulum in the model is chosen so that M_z from the pendulum model approximately matches the M_z from the CFD model. The CFD model sums the moments about z at *a*=0 and *t*=0. The CFD model's origin is located at the top of the tank. The pendulum model uses the same coordinate system.

The magnitude of the static mass, m_0, and the static mass location, h_0, are calculated using Equation 9 and Equation 10, respectively. The center of mass location of the fully-settled propellant, h_T, and total mass, m_T, are taken from the CFD model results.

$$m_0 = m_T - m$$

Equation 9

$$h_0 = \frac{m_T h_T - m h_p}{m_0}$$

Equation 10

The equations can be modified to find results for a multiple pendulum model. To find the forces and moments, the forces and moments from each individual pendulum are added together. To find the static mass magnitude, m is replaced with $(m_1 + m_2 \ldots + m_n)$ in Equation 9. To find the static mass location, mh_p is replaced with $(m_1 h_{p1} + m_2 h_{p2} \ldots + m_n h_{pn})$ in Equation 10.

The static mass is treated as both a point mass and a body with a moment of inertia about its center of mass. This approach is necessary so that the pendulum model's total moment of inertia is equal to the propellant's moment of inertia when the propellant is in a settled 1-g configuration, I_{prop}. While during sloshing the moment of inertia of the body will change due to the change of shape due to sloshing, the settled 1-g propellant configuration is an adequate approximation.

$$I_{prop} = I_{propCM} + m_T D_{prop}^2$$

Equation 11

I_{propCM} is the moment of inertia of the propellant about its center of mass, outputted by CFD. D_{prop} is the distance between the propellant center of mass and the static mass location. Equation 11 is the parallel axis theorem, used to calculate the moment of inertia of the propellant mass about the static mass location. The pendulum mass moments of inertia, I_m, are calculated about the static mass location using Equation 12, where D_m is the distance between the pendulum mass and the static mass.

$$I_m = m D_m^2$$

Equation 12

Using a two-pendulum model, Equation 13 shows the equation for calculating I_{m0cm}, the moment of inertia of the static mass about its own center of mass, where the subscripts 1 and 2 refer to the two pendulums, respectively.

$$I_{m0cm} = I_{prop} - m_1 D_{m1}^2 - m_2 D_{m2}^2$$

Equation 13

Since the pendulums, when resting, are aligned with the center-line of the tank, the moment of inertia of the pendulums are zero when calculated about the center-line of the tank.

Basis for Two-Pendulum Model

NASA's Cassini mission used PMD propellant tanks similar to those on Europa Clipper, and also used a two-pendulum model for slosh analysis. A notional tank and PMD is shown in Figure 4.

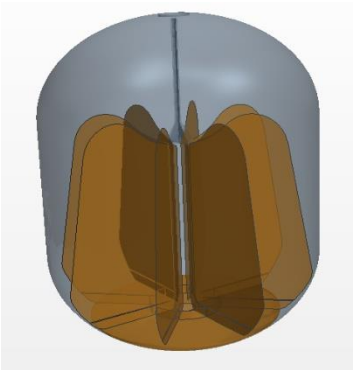

Figure 4. Notional tank and PMD

In a paper written by Enright and Wong on Cassini slosh analysis (Enright, 1994), the authors used two separate pendulums to model two modes of propellant sloshing, which they called "sector" and "full" tank slosh modes. They base this on the observation that the tank geometry produced by the PMD can be approximated as both a sector of a cylinder and an annular cylinder, as shown in Figure 5. The two pendulums in the model account for the two slosh modes between the PMD vanes and around the PMD vanes.

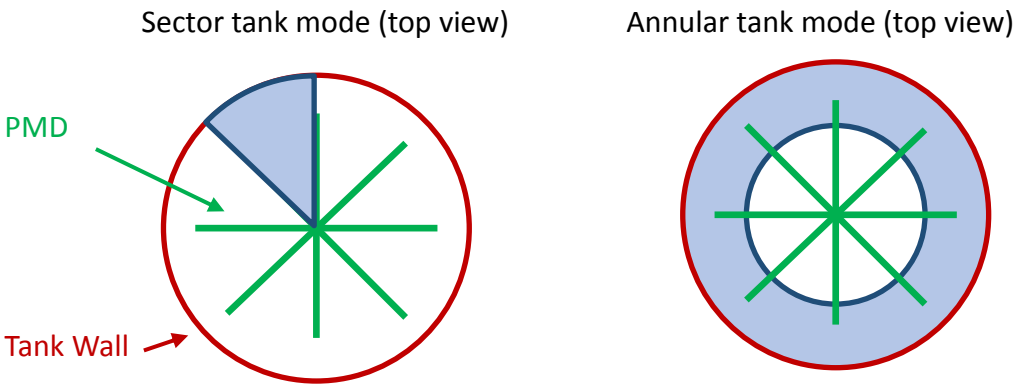

Figure 5. Schematic of PMD approximated as annular and sector tank modes.

Extensive analytical and experimental work was conducted on liquid sloshing in simple geometry tanks including cylindrical sector and annular tanks. Much of this work was compiled in NASA's technical report SP-106 (Abramson, 1966), and updates were later added by the Southwest Research Institute (SwRI) (Dodge, 2000). These documents have been used extensively in the past by slosh analysts. They documents provide analytical equations for frequency associated with each of these slosh modes, which are used later as a sanity check to validate the model parameters. Additionally, equations from these documents for damping ratio in a bare cylindrical tank were used as a comparison for model parameters.

METHODOLOGY

High Level Summary

The goal was to find the parameters of two damped pendulums and one static mass that, when superimposed to calculate a total CM, most closely matched the CFD CM over time. This was done for two propellants at three fill fractions each, with the goal of selecting parameters that were monotonic as a function of fill fraction to allow for interpolation between fill fractions. The behavior before the first peak (the first wave of movement from one side of the tank to the other) experienced highly nonlinear damping, so a pendulum model was not able to capture the behavior before the first peak while also accurately modeling the behavior after this first peak. Therefore, the decision was made to fit the pendulum model to the behavior after the first peak only. It will be shown later that this is a conservative choice for all initial offset angles greater than the 15-degree offset used in the CFD simulations.

Examination of the CFD CM data reveals that it can be approximately resolved into the sum of two separate damped oscillations. Initial guesses for each pendulum's frequency ω and damping ratio ζ were calculated by selecting points in the CFD data that were approximately the peak-to-peak values for each pendulum. A mass fraction *mf* was defined to describe the pendulum bob mass as a fraction of the total propellant mass. Then, the first pendulum's mf_1, ω_1, and ζ_1 were generated using curve fitting to the CFD CM data. The second pendulum's mf_2, ω_2, and ζ_2 were generated by curve fitting to the difference between CFD CM data and the first pendulum's CM contribution. Additional steps were taken to fine-tune the parameters to improve the fit and minimize the error in force. Pendulum attachment height *h* was found by minimizing the error in moment. Finally, moments of inertia I_a and I_z were assigned to the static mass to have the model reflect the total moment of inertia of the settled fluid.

Initial Guesses

Figure 6 shows an example of the CFD CM data and the peaks used to find initial guesses for ω (used along with acceleration to calculate *length*) and ζ.

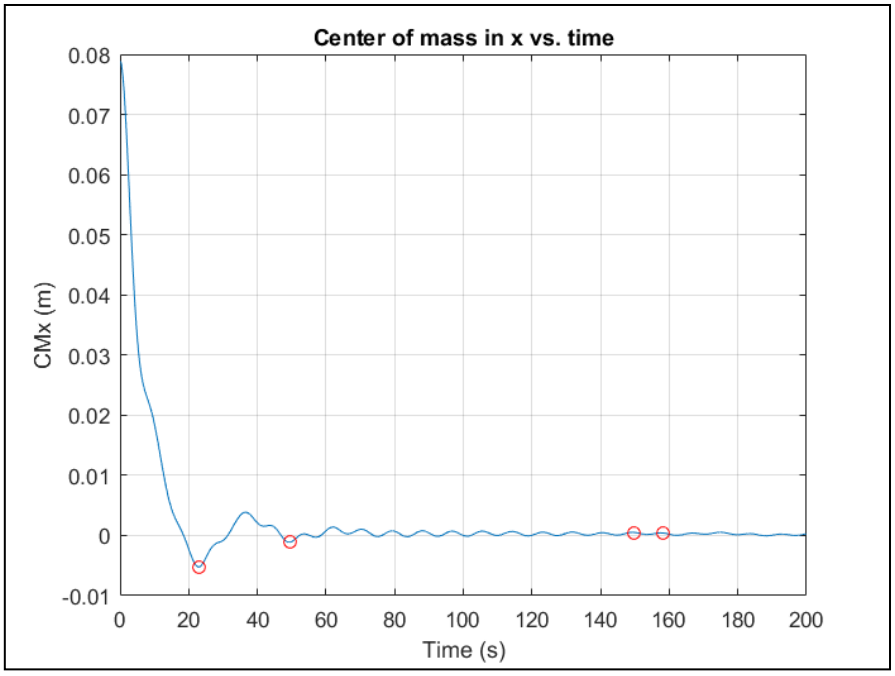

Figure 6. CFD CM data with peaks indicated.

The first set of consecutive peaks is selected at the beginning of the simulation where the longer pendulum's movement dominates the CM movement. Equation 14 and Equation 15 are used to calculate ω_1 and ζ_1 from these points. The second set of consecutive peaks is selected near the end of the simulation, after the longer pendulum has damped out and the shorter pendulum's movement dominates the CM movement. ω_2 and ζ_2 are calculated from these points. In some data sets, the CFD CM oscillates about a non-zero center. This offset is on the order of 1 mm or less and is likely due to numerical error in the simulation. To center these data sets about zero for the initial guess calculation, the average CM of the last few seconds was subtracted from every point in the CM data.

$$\omega = \frac{1}{T_2 - T_1}$$

Equation 14

$$\zeta = \frac{1}{\sqrt{1 + \left(\frac{2\pi}{\delta}\right)^2}} = \frac{1}{\sqrt{1 + \left(\frac{2\pi}{\ln(CM_1/CM_2)}\right)^2}}$$

Equation 15

T_1 and T_2 are the times of the first and second consecutive peaks, respectively, CM_1 and CM_2 are the center of masses of the first and second consecutive peaks, respectively, and δ is the logarithmic decrement.

Curve Fitting Pendulum Equation

Matlab's curve-fitting fsolve function was used to iteratively solve for a more accurate mass fraction *mf,* frequency ω, and damping ratio ζ that would allow the pendulum model to fit the CFD data. The initial guesses passed into fsolve were 0.5 for *mf*, and the previously generated initial guesses for ω and ζ. The equation passed to fsolve was Equation 16, where *m* was the mass of the pendulum bob, m_t was the total mass of the propellant, *L* was the length of the pendulum, and θ was the angle of the pendulum over time given in Equation 4.

$$CMx(t) = \frac{m}{m_t} CM_1(t) = \frac{m}{m_t} L \sin(\theta(t))$$

Equation 16

fsolve was used first to fit a longer pendulum to the high-amplitude oscillation, as shown in Figure 7. The blue circles indicate the points of interest where fsolve aimed to match the pendulum's CM contribution with the CFD CM. The points were selected to span the time starting at the first peak and ending when the oscillation appeared to damp out completely.

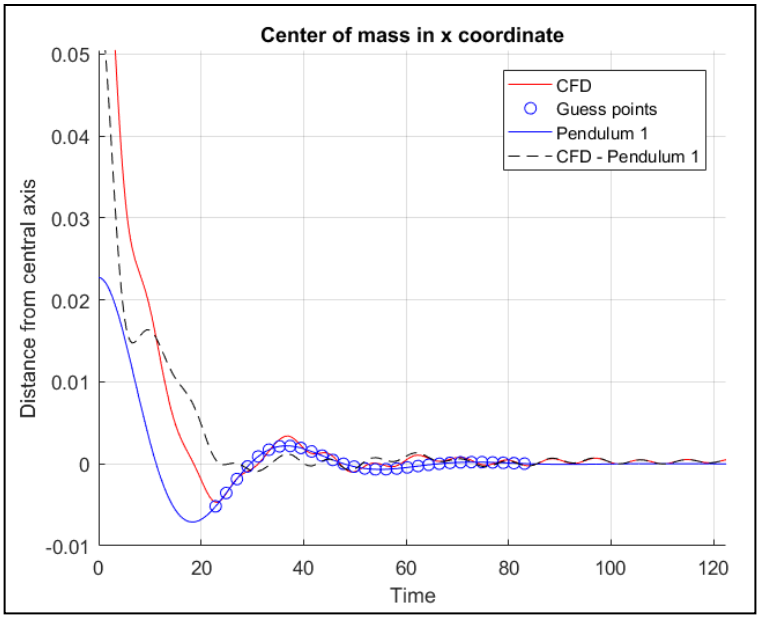

Figure 7. Long pendulum fit to CFD CM data.

Then, fsolve was used to match a second pendulum to the difference between the first pendulum's CM contribution and the CFD CM. The difference is shown in black in Figure 8. The

points of interest here were selected in a time interval where the difference is close to the shape of a damped sinusoid.

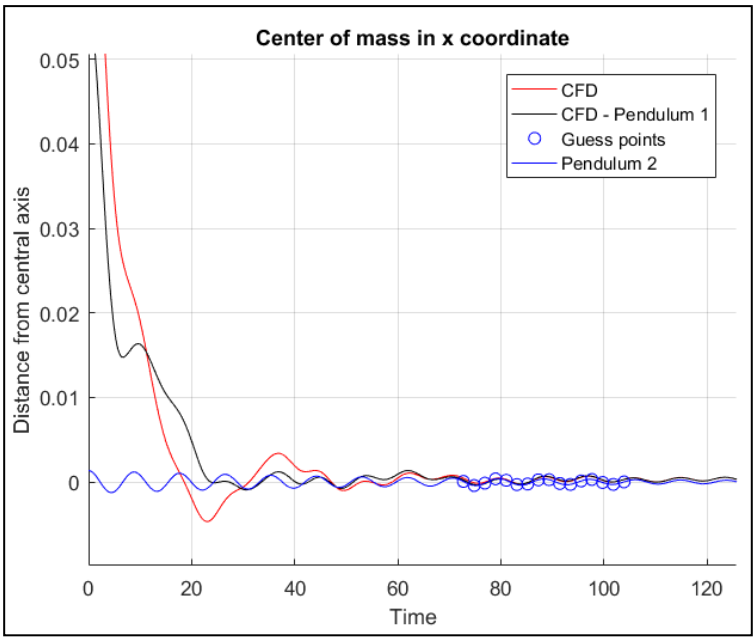

Figure 8. Short pendulum fit to the difference between CFD CM and the long pendulum's CM component.

For both pendulums, trial and error was required to find the points of interest that allowed fsolve to produce an accurate fit. This included changing the time interval or the timestep between points. For the shorter pendulum especially, it was often necessary to subtract a correction factor to center the CFD oscillations about zero.

After mf, ω, and ζ were determined for both pendulums, a total CM was calculated by taking the sum of Equation 16 for both pendulums.

Iterations to find mass participation fractions

For some test cases, it was possible to further improve the pendulum fit by iterating on the mass fraction parameter. The underlying reasoning is that if the model were perfect, then when one pendulum was passing through vertical, the other pendulum's CM contribution would account for the entire CFD CM of the fluid. Using this reasoning, several points of interest were selected where the first pendulum was vertical. This happens when the first pendulum's CM contribution crosses zero (intercepting the time axis). In Figure 9, the black x's are points where Pendulum 2's CM crosses zero; so if the model were perfect, Pendulum 1 would equal CFD.

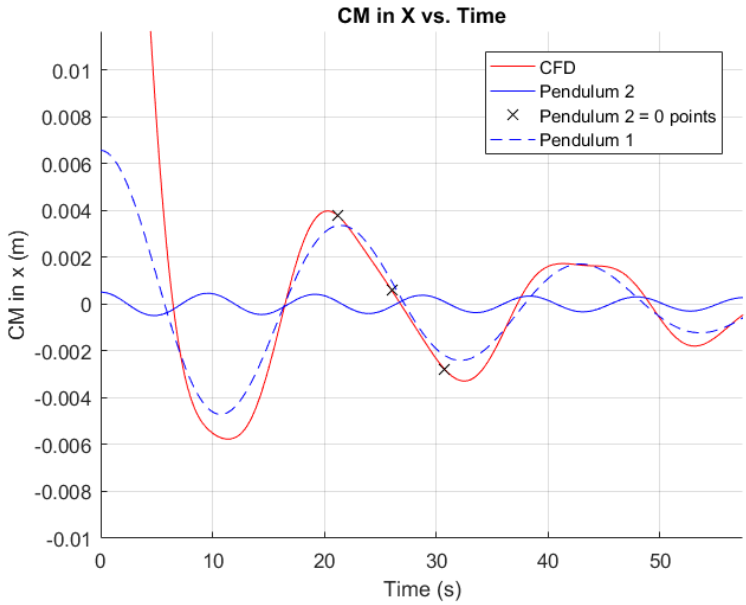

Figure 9. Points of interest for iterating on mass fraction.

Then, Equation 17 was used at each of these points to calculate the mass fraction required of the second pendulum to match the CFD CM. These mass fractions were averaged and used as the new parameter for the next iteration. The same calculation was carried out for points of interest where the CM of the second pendulum crossed zero. Iterations were performed until the mass fractions converged or it became clear that they would not converge.

$$mf_2 = \frac{CMx}{L_2 \sin\theta_2}$$

Equation 17

Additional Fine-Tuning

After using curve fitting to obtain a full set of parameters for each propellant at each fill fraction, the parameters were fine-tuned to improve the fit and meet certain criteria. The following adjustments were only used in cases where minor adjustments could achieve the criteria without compromising the quality of fit. The values for m, ω, and ζ were adjusted to be monotonic as a function of fill fraction. The values for m and ω were adjusted to be identical between the two different propellants. The plot of the model vs. the CFD data was examined closely to adjust the parameters to fit the peaks more accurately. The final model for 50% fill fraction is shown in Figure 10.

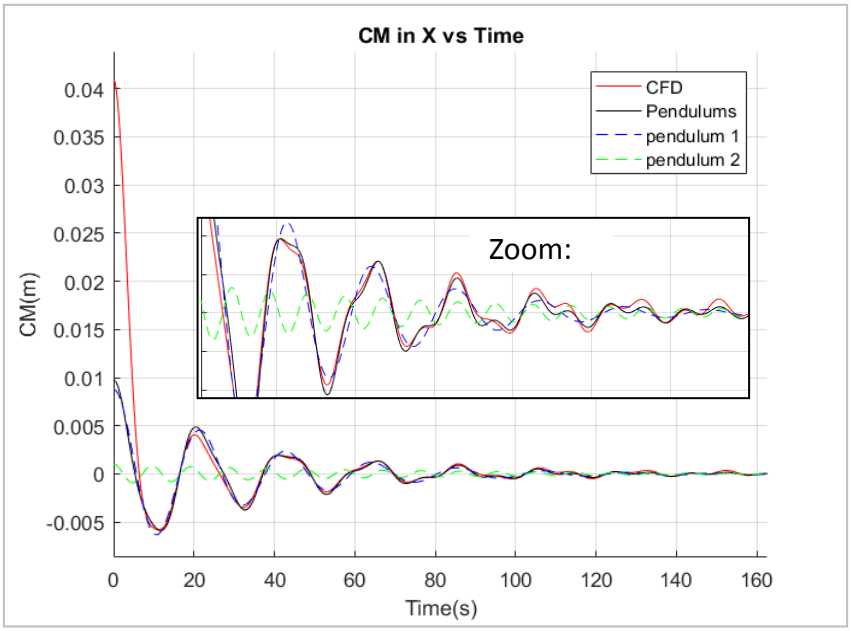

Figure 10. Pendulum model vs. CFD CM at 50% fill fraction.

Quantifying Accuracy of Fit

The metric used to quantify the accuracy of the model was the mean difference between pendulum force and CFD force. This was calculated using Equation 18, where *n* is the number of points in the range of interest. The black arrows in Figure 11 show the force errors that were averaged.

$$\frac{1}{n}\sum_{1}^{n} abs(CFD - pendulum)$$

Equation 18

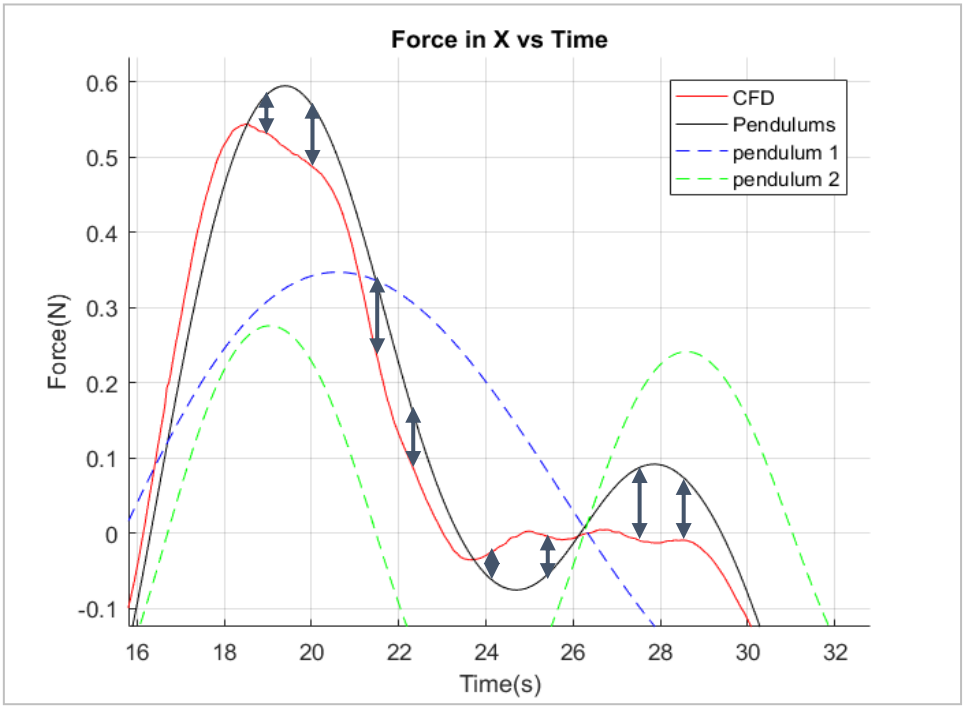

Figure 11. Illustration of error in force.

It is important to note that a slight time shift between the CFD peaks and pendulum model peaks can lead to a misleadingly high error. A visual inspection of the matching between the CFD and pendulum outputs was done as an added check to ensure a good fit.

Finding Pendulum Attachment Point

The "hinge height" is the point along the tank's central axis where the pendulum string should be attached to most accurately model the moment exerted by the fluid. Equation 8 is rewritten as Equation 19 to include hinge height *h* as a variable.

$$M_z = F_t l_a + F_a l_t$$
$$= \left(ml\,\dot{\theta}^2 \sin\theta - ml\,\ddot{\theta}\cos\theta\right)(-(h - l\cos\theta)) + (-ml\dot{\theta}^2\cos\theta - ml\ddot{\theta}\sin\theta - mg)(l\sin\theta)$$

Equation 19

$$M_{z_{total}} = M_{z_1} + M_{z_2}$$

Equation 20

Initially, an attempt was made to use fsolve to fit a curve to the CFD moment data while allowing h_1 and h_2 to vary. However, this method did not result in a good fit. Instead, h_1 was varied by manually inputting different values. The value was selected that minimized the mean error in moment (calculated using the same method as mean error in force in the previous section). This process was then repeated for h_2. In some cases, the optimized hinge heights resulted in the pendulum bob being outside the physical confines of the tank walls, and the hinge height was adjusted slightly to avoid this, but only if quality of fit was not significantly impacted. An example of the pendulum bob inside the tank walls is shown in Figure 12.

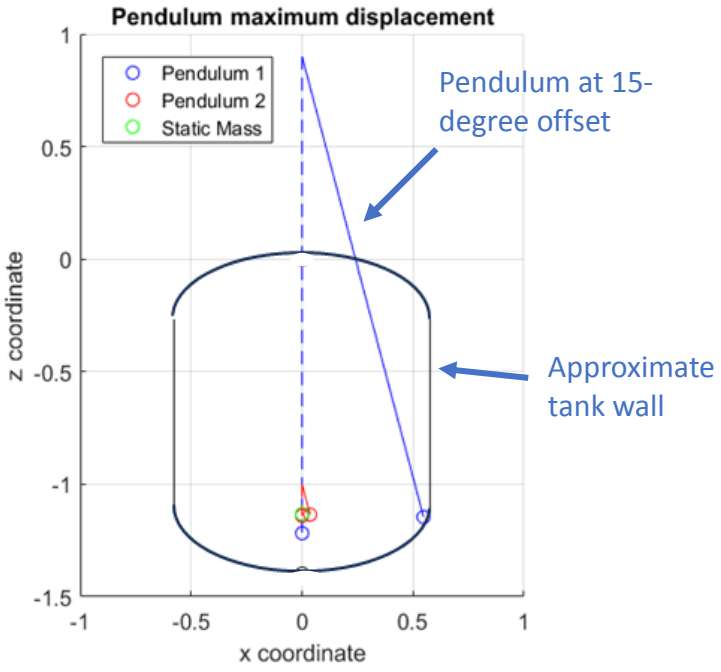

Figure 12. Pendulums at maximum displacement within tank walls.

Finding Static Mass Moment of Inertia

In order to accurately model the total moment of inertia of the propellant, a moment of inertia is assigned to the static mass, as described in the theory section. This calculation used the settled state of the propellant and pendulums and the reference point was the center of mass

of the settled propellant. The static mass's moment of inertia about the axial axis is equivalent to the settled propellant's moment of inertia about the axial axis (calculated using CFD). The static mass's moment of inertia about the *z*-axis is given by solving for $I_{mstatic}$ in Equation 21. Again, the *z*-axis is the direction orthogonal to both the tank's vertical axis and the lateral sloshing axis.

$$I_{settled\ propellant\ about\ propellant\ CM} = I_{\text{"settled" pendulm model about propellant CM}}$$
$$= m_1\left((H_1 - l_1) - CM_{prop}\right)^2 + m_2\left((H_2 - l_2) - CM_{prop}\right)^2$$
$$+ \left(I_{mstatic} + m_0\left(H_{static} - CM_{prop}\right)^2\right)$$

Equation 21

Figure 13 illustrates the variables in Equation 21.

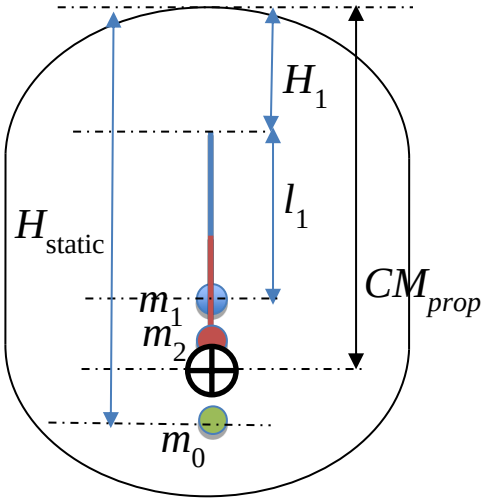

Figure 13. Schematic of tank with settled pendulums.

RESULTS AND DISCUSSION

Results

Table 1 below outlines each of the CFD cases that were run. Cases 1-3 represent different fill fractions of NTO and Cases 2-6 represent different fill fractions of MMH. The 2_θ cases are the test cases in which Test 2's CFD surface offset angle is changed to θ. These cases are not used in determining trends as a function of fill fraction, but give essential insight into the limits of the pendulum models.

Table 1. High-g Slosh Test Cases for November 2016 Europa Slosh Deliverable

Case	Acceleration (m/s)	Temperature (deg C)	Initial Offset Angle (deg)	Fill Fraction (%)	Mass (kg)	Propellant
1	0.071	15	15	25	418.6	NTO
2	0.057	0	15	50	855.5	NTO
3	0.039	0	15	85	1454.3	NTO
4	0.071	15	15	25	252.6	MMH
5	0.057	0	15	50	513.3	MMH
6	0.039	0	15	85	872.6	MMH
2_10	0.057	0	10	50	855.5	NTO
2_5	0.057	0	5	50	855.5	NTO
2_30	0.057	0	30	50	855.5	NTO

The pendulum parameters derived for these cases are listed below in Table 2. These parameters prioritized fitting the CFD slosh behavior after the first CM peak and ignored the behavior before the first peak. The Methodology section discusses the reasoning for fitting only one of these regions.

Table 2. Pendulum Model Parameters for Different Test Cases, Fitting After First Peak

	Test Case Number					
	1	2	3	4	5	6
Propellant	NTO			MMH		
Fill Fraction (%)	25	50	85	25	50	80
Accel (m/s^2)	0.071	0.057	0.039	0.071	0.057	0.039
m_1 (kg)	20.09	44.49	210.87	12.12	26.69	126.53

m_2 (kg)	12.56	24.81	26.18	7.58	14.89	15.71
m_0 (kg)	385.95	786.20	1217.25	232.90	471.72	730.3662
mf_1 (kg)	0.048	0.052	0.145	0.048	0.052	0.145
mf_2 (kg)	0.03	0.029	0.018	0.03	0.029	0.018
mf_0 (kg)	0.922	0.919	0.837	0.922	0.919	0.837
h_1 (m)	0.9	-0.4	-0.5	0.9	-0.5	-0.5
h_2 (m)	-1.0	-0.7	-0.3	-0.9	-0.7	-0.2
h_0 (m)	-1.12	-0.99	-0.79	-1.14	-0.99	-0.8
l_1 (m)	2.118	0.651	0.353	2.118	0.651	0.353
l_2 (m)	0.140	0.132	0.301	0.140	0.132	0.301
ξ_1	0.340	0.105	0.035	0.350	0.110	0.037
ξ_2	0.015	0.022	0.035	0.020	0.025	0.037
f_1 (Hz)	0.029	0.047	0.053	0.029	0.047	0.053
f_2 (Hz)	0.113	0.105	0.057	0.113	0.105	0.057
$I_{z-static\ mass}$ (kg-m^2)	32.52	88.89	224.06	19.82	52.88	133.75
$I_{a-static\ mass}$ (kg-m^2)	55.97	128.54	228.64	33.87	77.17	137.20

There is not a unique solution when curve fitting to the results. Parameters were chosen that provided a good fit, but since the pendulum model cannot match the results exactly, engineering judgment was used to determine what constituted a good fit. The propellant slosh before the first CM peak was ignored during the fitting process and thus is not reflected in the pendulum model.

Figure 14 through Figure 22 illustrate the quality of fit of the pendulum model for some of the test cases.

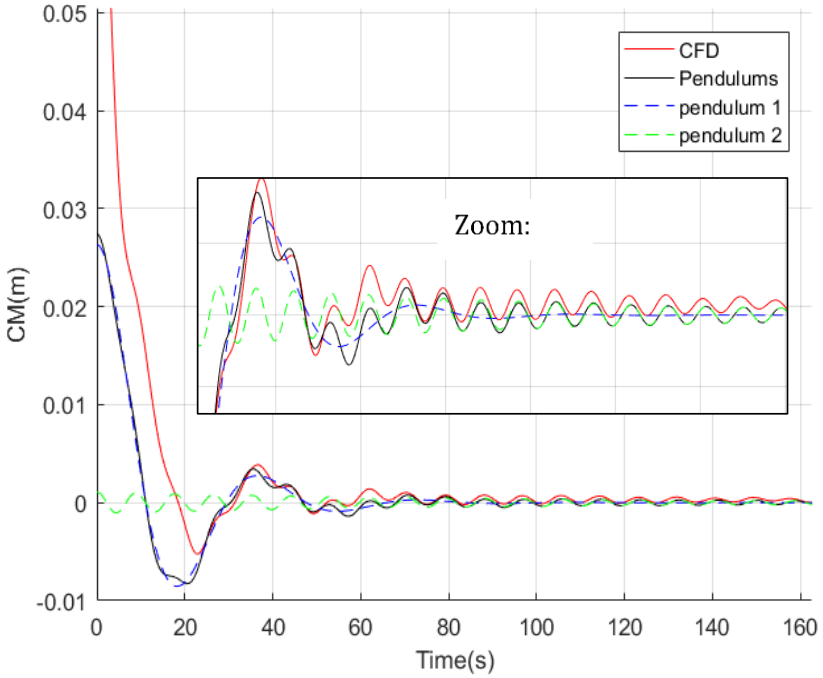

Figure 14. CM in transverse direction vs. time for 25% fill fraction.

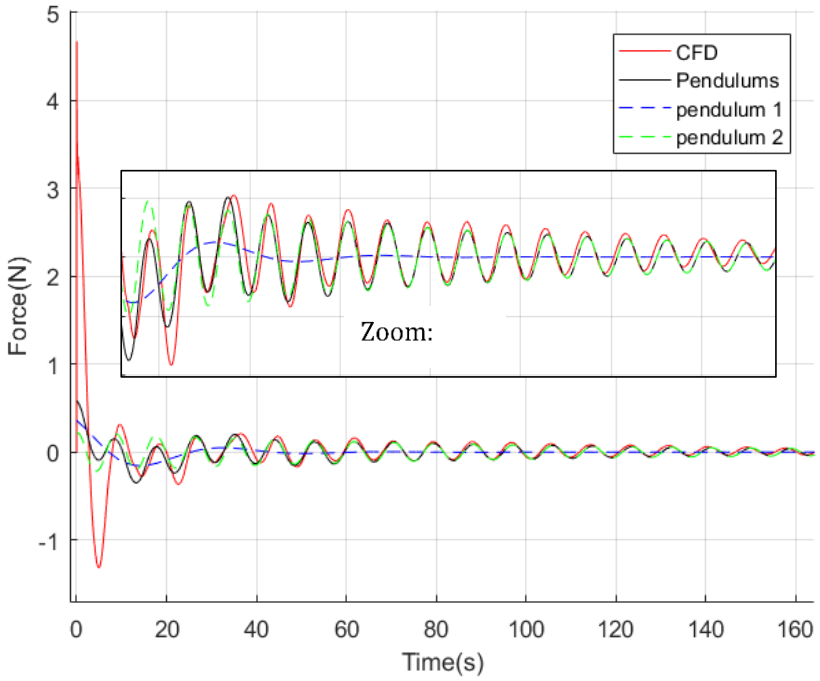

Figure 15. Force in transverse direction vs. time for 25% fill fraction.

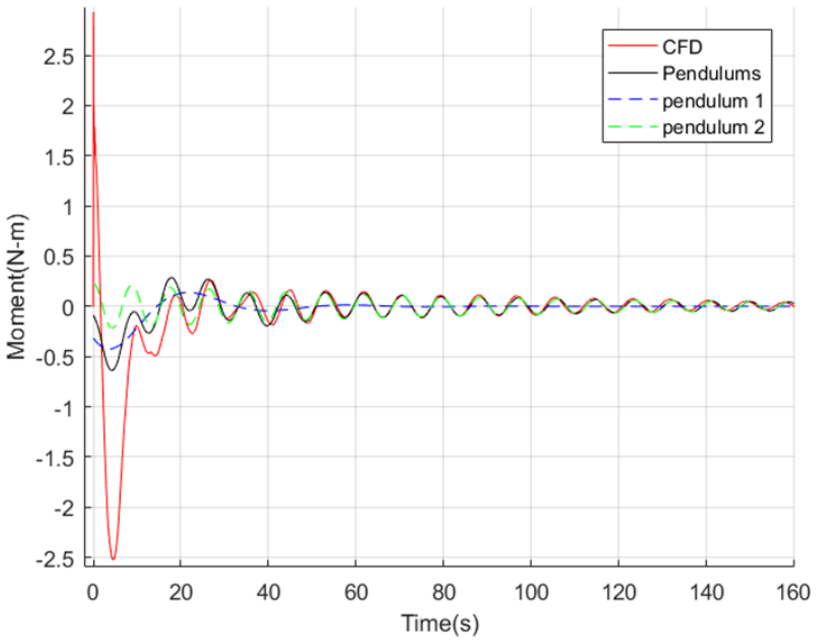

Figure 16. Moment about z-axis vs. time for 25% fill fraction.

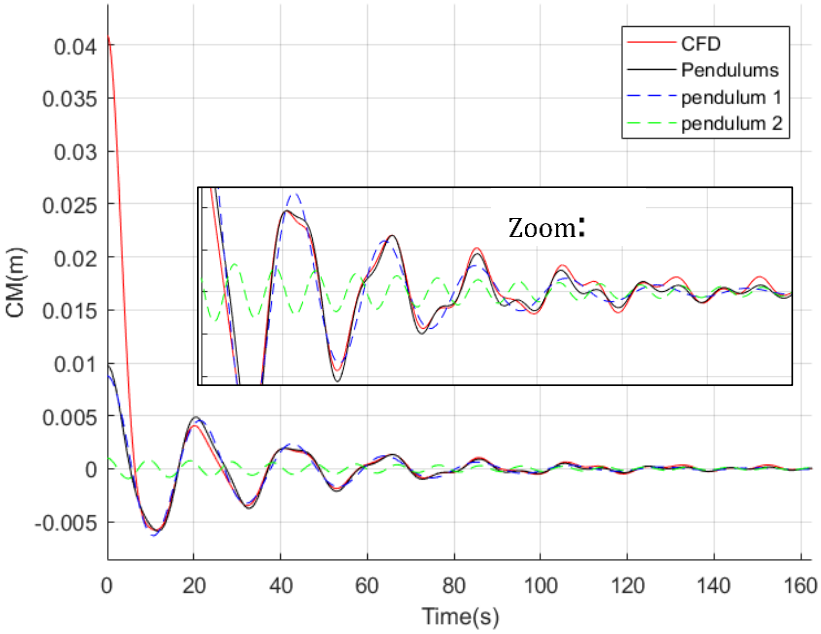

Figure 17. CM in transverse direction vs. time for 50% fill fraction.

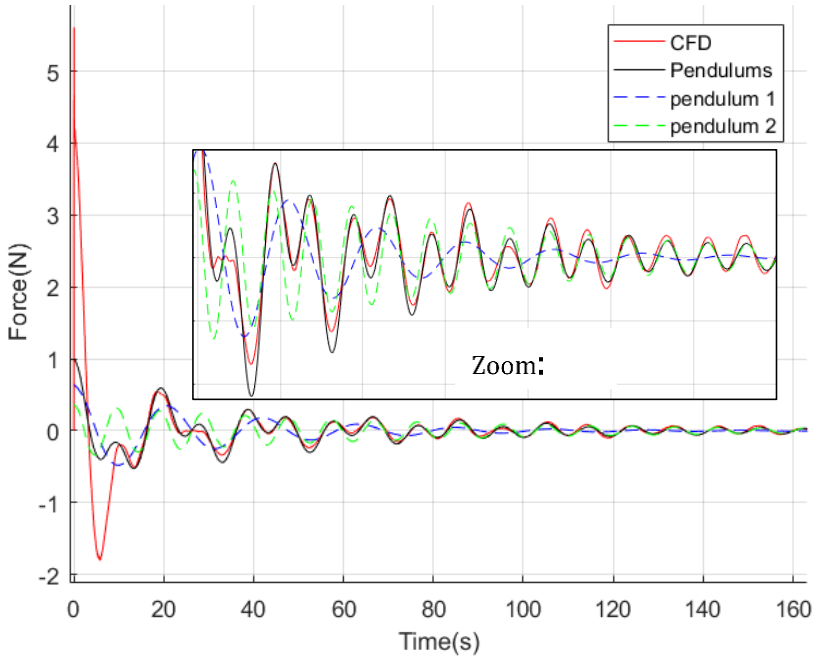

Figure 18. Force in transverse direction vs. time for 50% fill fraction.

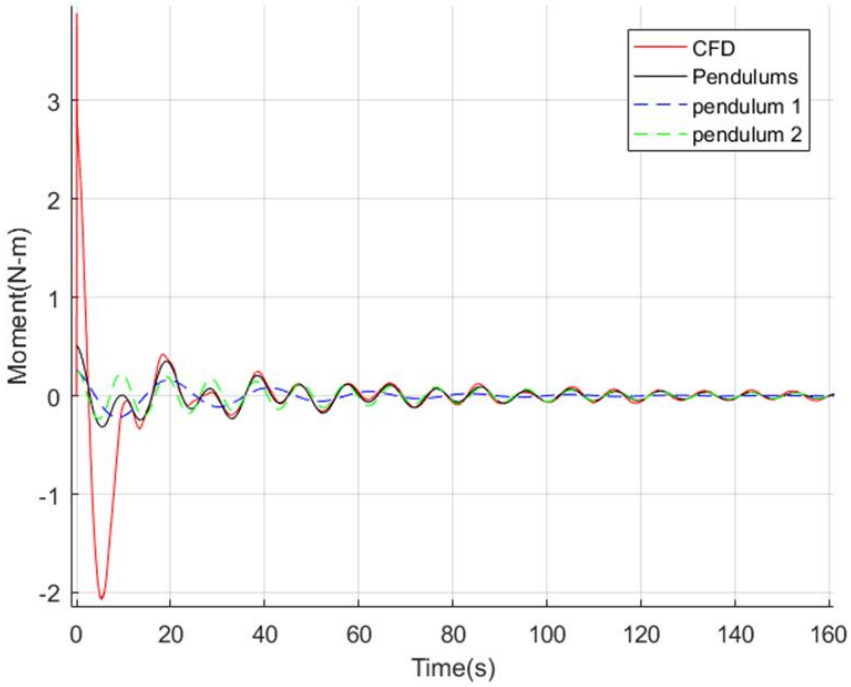

Figure 19. Moment about z-axis vs. time for 50% fill fraction.

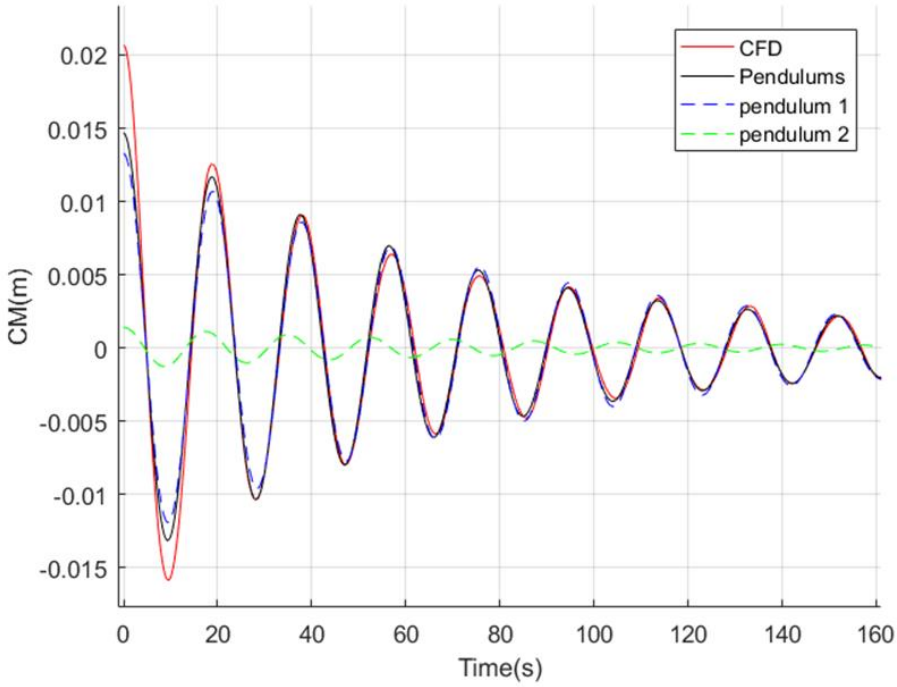

Figure 20. CM in transverse direction vs. time for 80% fill fraction.

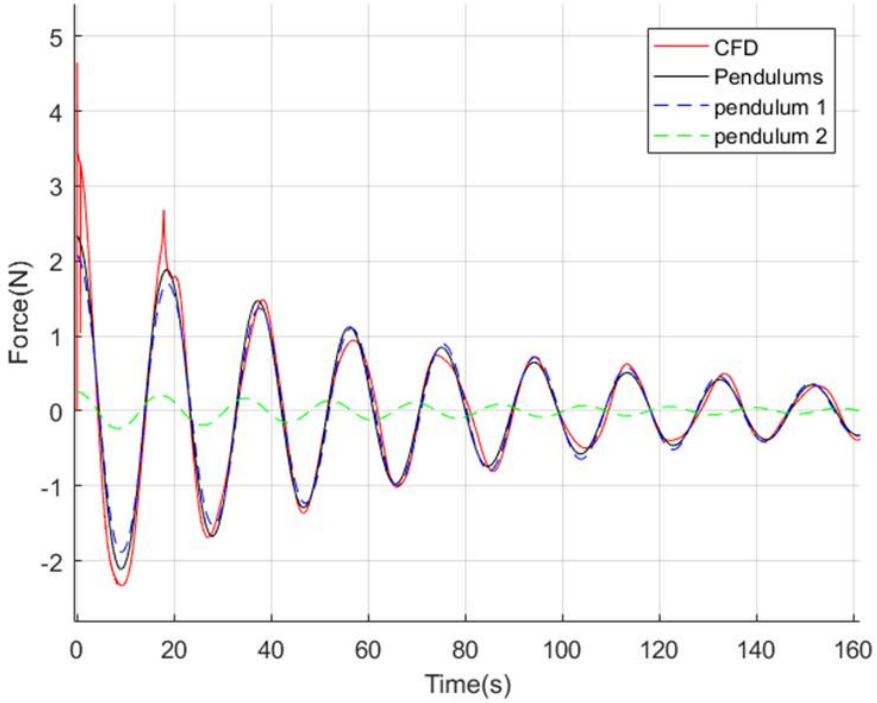

Figure 21. Force in transverse direction vs. time for 80% fill fraction.

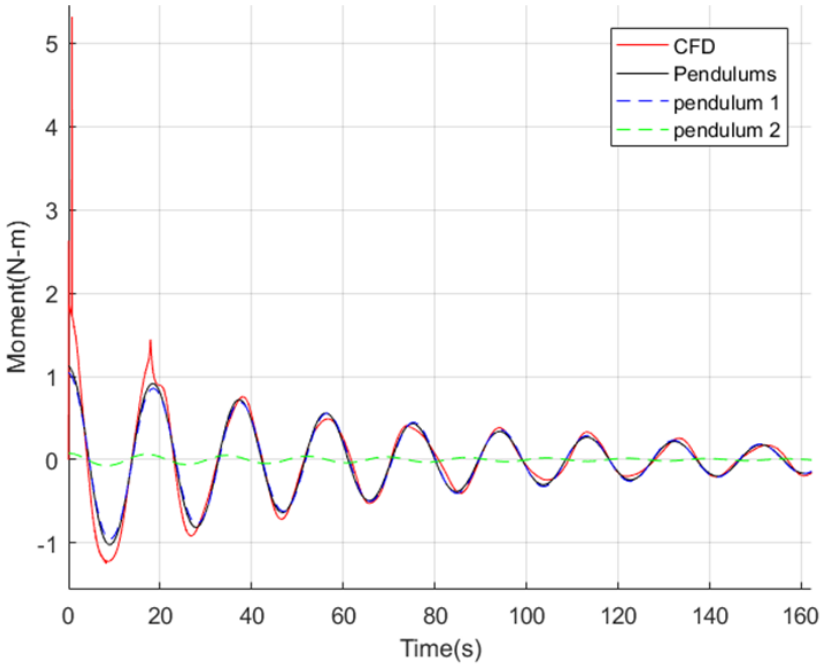

Figure 22. Moment about z-axis vs. time for 80% fill fraction.

Discussion of Trends and Literature Comparison

The pendulums' mass, frequency, damping ratio, and hinge height were plotted as a function of fill fraction to examine the trends. These trends were compared to analytical and experimental trends for simpler tank geometries presented by Abramson (1966), Enright (1994), and Dodge (2000).

Figure 23 shows that the pendulum bob mass fractions are monotonic as a function of fill fraction. It was found that identical mass fractions for NTO and MMH at a given fill fraction were able to accurately model both propellants. The trend indicates that for interpolating between fill fractions, a piecewise linear fit would be more accurate than a linear fit. The physical reasoning for this is that for the first two fill fractions, the PMD is partially covered by the propellant (see Figure 1), so sloshing occurs primarily between the vanes. For the last fill fraction, the PMD is completely covered, so a different slosh behavior occurs above the PMD.

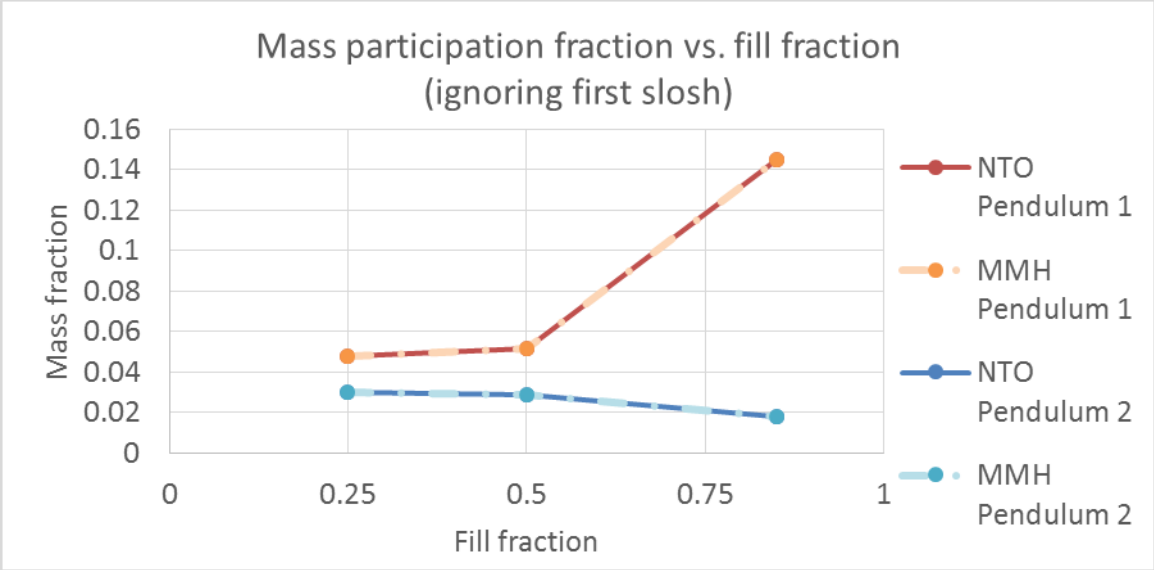

Figure 23. Mass fraction as a function of fill fraction.

Figure 24 plots pendulum frequencies as a function of fill fraction, which are also monotonic as a function of fill fraction. As with mass fraction, it was found that identical frequencies for NTO and MMH at a given fill fraction was able to accurately model both propellants. Also shown in Figure 24 are analytical frequencies in a "bare tank" (cylindrical flat-bottomed tank with no PMD) given by the equation in Section 3.2 of Dodge (2000). A comparison of the two pendulum frequencies to the bare tank frequency was also included for a slightly different tank geometry in the Cassini mission (Enright, 1994), shown here as Figure 25. Both plots show the two pendulum frequencies converging to the bare tank frequency as fill fraction increases. The physical explanation for this is that as the fill fraction increases, the PMD becomes fully covered by the propellant, so the slosh behavior begins to resemble that of a bare tank with no PMD.

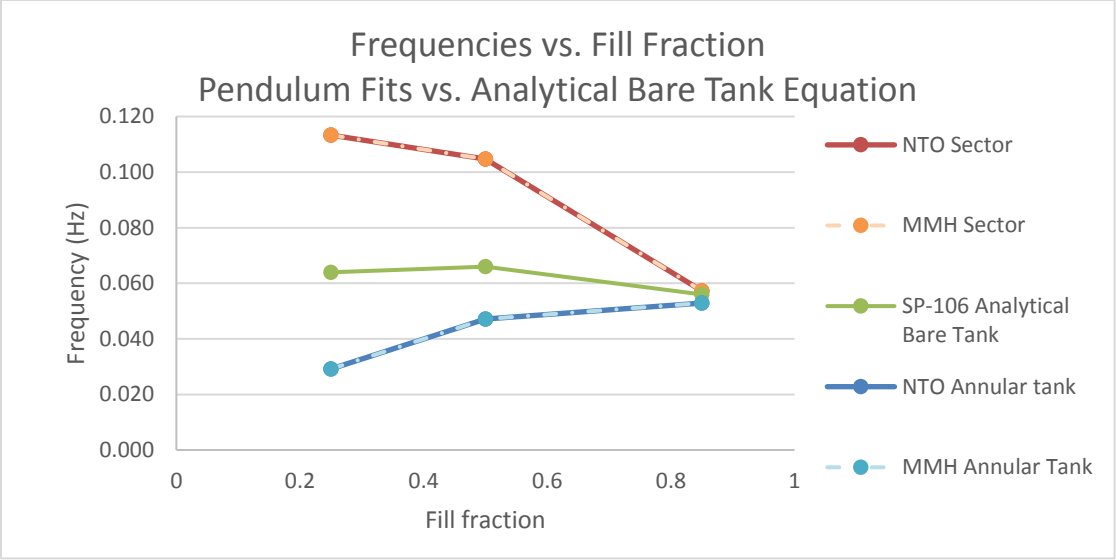

Figure 24. Frequency vs. fill fraction compared to analytical bare tank.

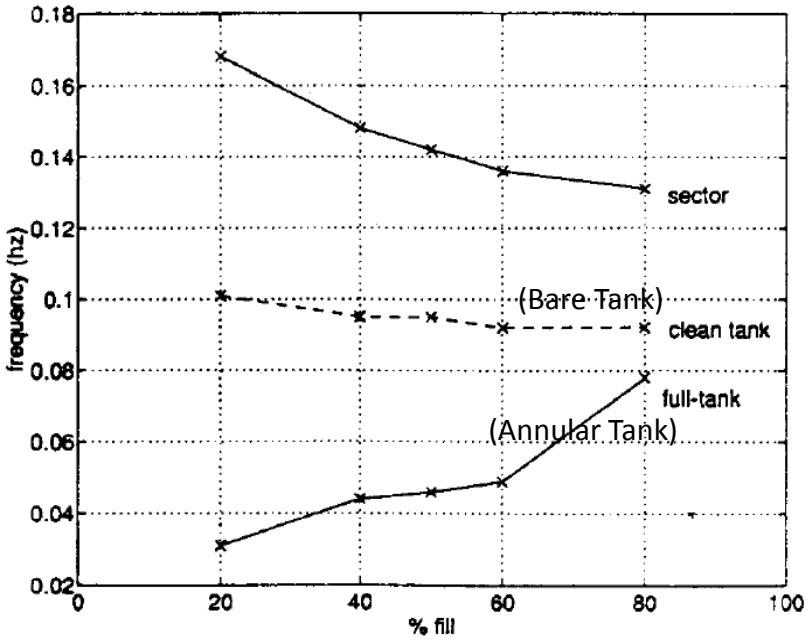

Figure 25. Cassini frequency as a function of fill fraction (Enright, 1994).

Abramson (1966) provided analytical equations for sector and annular frequencies in a cylindrical tank in *SP-106*. Figure 2.3 in Section 2.3 of *SP-106* shows how *h*, *a*, *b*, and α are derived from the geometry of the sector or annular tank. Equation 2.19 in Section 2.3 of *SP-106* shows the equation for slosh frequency as a function of acceleration, fluid height, and tank geometry, copied here as **Error! Reference source not found.**. *g* is the acceleration. The coefficient ζ_{mn} in this equation is tabulated by Bauer (1963) and is dependent on tank

geometry. The subscript *m* is 1 for the mode of interest, as explained by Dodge (2000) Section 1.5.

$$\omega = \sqrt{\zeta_{\mathrm{mn}} \frac{g}{a} \tanh\left(\zeta_{\mathrm{mn}} \frac{h}{a}\right)}$$

Equation 22

Table 3 summarizes the variables used in Equation 22 to calculate frequencies.

Table 3. Parameters Used in Analytical Sector and Annular Frequencies

Parameter	**Sector Slosh**	**Annular Slosh**
a (m)	Radius of tank	Radius of tank
b (m)	0	Average radius of PMD vane
α	1/8	1/2
p	$\frac{m}{2\alpha}$	$\frac{m}{2\alpha}$
k	*b/a*	*b/a*
ζ_{10}	Look up from Bauer (1963) tables	Look up from Bauer (1963) tables

The analytical sector and annular frequencies calculated using this equation were plotted in Figure 26 and compared to the pendulum model frequencies. The plot shows that the pendulum frequencies and analytical frequencies are close. The physical reason for the differences include the fact that the PMD is neither a true sector nor annular tank, which will affect all fill fractions. The inner radius of the annular tank was approximated as an average radius of the PMD vane, but the PMD shape is not physically representative of an annular tank.

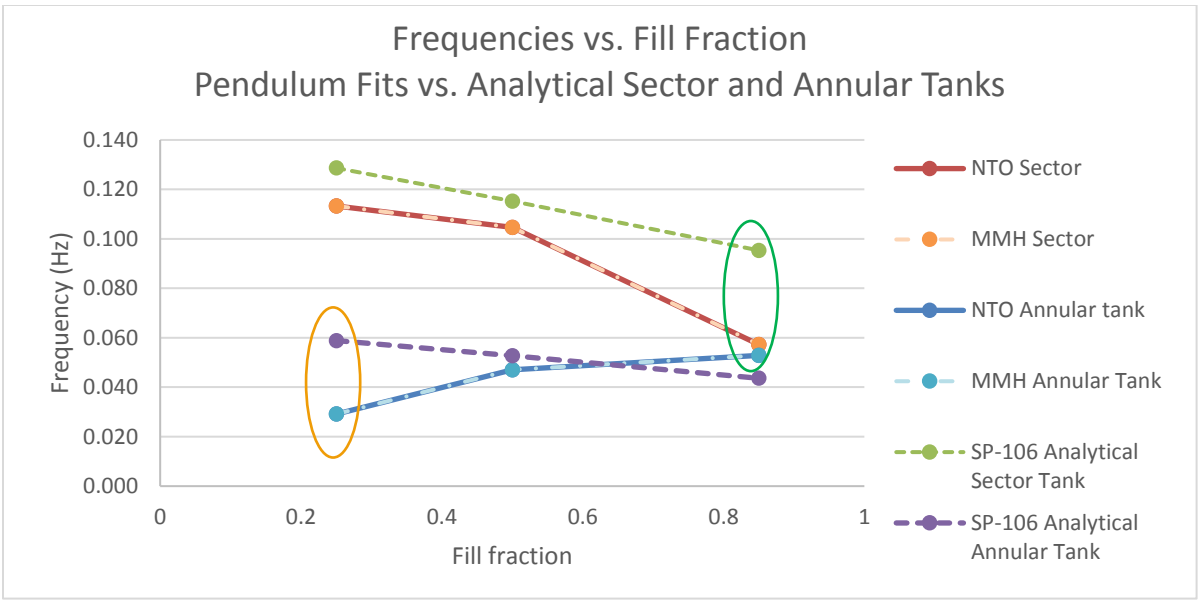

Figure 26. Frequencies as a function of fill fraction compared to analytical sector and annular tanks.

There was a larger discrepancy in pendulum and analytical annular slosh frequencies at 25% fill (circled in yellow). This was likely due to the fact that the CFD data came from a domed bottom tank, while the analytical equation was for a flat-bottomed tank. At 25% fill, the propellant is almost entirely sloshing in the domed section, so that geometry difference will affect the frequencies more than at higher fill fractions. There was also a larger discrepancy in the sector slosh at 85% fill (circled in green). This was likely due to the PMD being fully covered by the propellant at this fill fraction. The sloshing occurred above the PMD where the tank geometry is similar to a bare cylinder without vanes to form sectors.

Damping ratio trends were also validated against correlations given in literature. Dodge (2000) Section 2.2 includes a correlation equation for damping ratio in a bare cylindrical tank (no sectors or annulus) as a function of geometry, fluid height, and acceleration. It was developed by Mikishev and Dorozhkin based on their experimental tests and copied here as Equation 23. It includes a correction coefficient C_{dome} to correct for a dome-bottomed tank, which can be read off a chart labeled Figure 2.2 in Dodge (2000), copied here as Figure 27. For the 25% fill fraction C_{dome} = 2 was used, and for 50% and 85% fill fraction, C_{dome} = 1 was used. These values for C_{dome}

correspond to liquid fill ratios of *h/R,* where *h* is the depth of the settled propellant from the end of the hemispherical bottom and R is the radius of the cylindrical portion of the tank.

$$\gamma = C_{dome} 0.79 \sqrt{Re_1} \left[1 + \frac{0.318}{\sinh\left(\frac{1.84h}{R}\right)} \left(1 + \frac{1 - \frac{h}{R}}{\cosh\left(\frac{1.84h}{R}\right)} \right) \right]$$

Equation 23

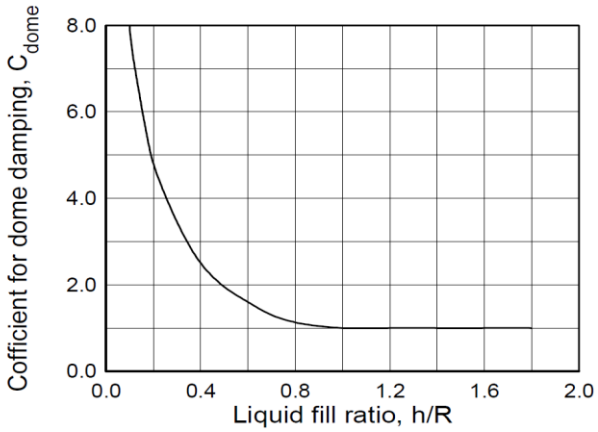

Figure 27. Correction coefficient for domed bottom tank.

Figure 28 shows damping ratios for each pendulum and the damping ratios given by Mikishev and Dorozhkin's correlation. The damping ratios of each pendulum were monotonic as a function of fill fraction. The more viscous propellant, MMH, has a slightly higher damping ratio than NTO. The damping ratios for two pendulums are somewhat close to the damping ratio in a bare tank, especially as the PMD becomes covered and the slosh behavior becomes more like sloshing in a bare tank.

The pendulum model's increase in damping due to increased viscosity (i.e. increase from NTO to MMH) is much less than what the analytical correlations would predict. This could be related to the fact that the damping caused by a PMD is dominated by a drag force, while the damping in a bare tank is dominated by viscous force. Since the PMDs are identical for the two propellants, the drag force is identical, and the change in viscosity has only a small impact on

the damping coefficient. This idea was based on Section 2.3 of Dodge (2000), in a discussion of damping by ring baffles.

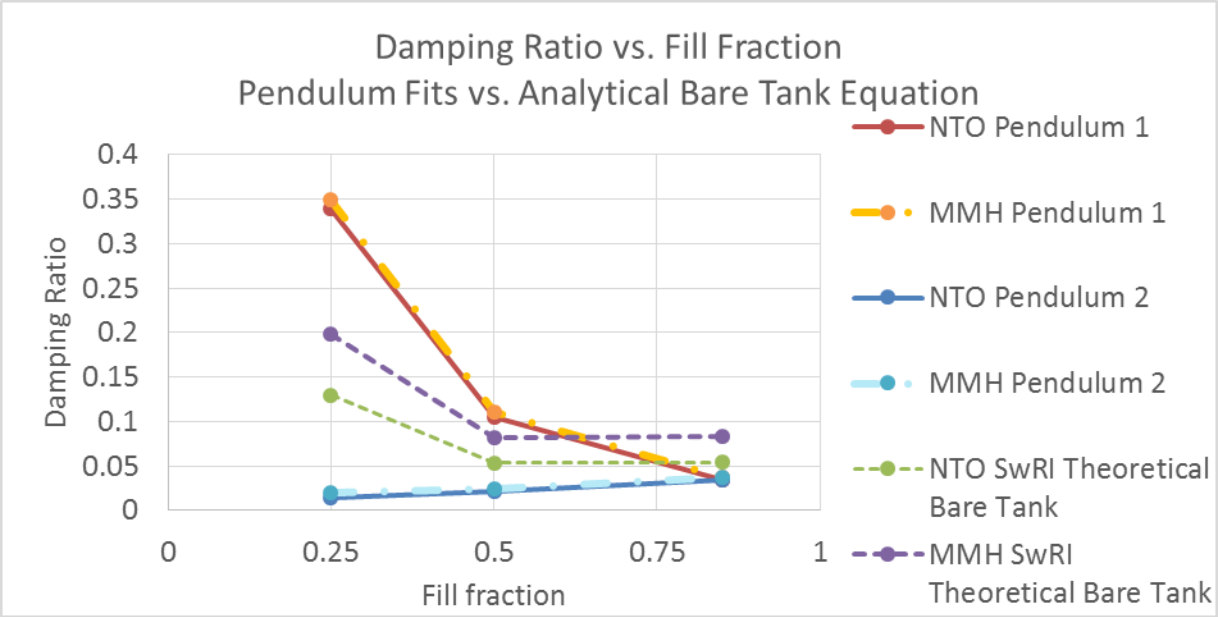

Figure 28. Damping ratio as a function of fill fraction compared to analytical.

Dodge (2000) presents an additional correlation by Stephens, et al. which yields similar bare tank damping ratios, but differs in that it doesn't provide a correction coefficient for the domed bottom. There was no analytical equation found for damping ratio in sector and annular tanks.

The final parameter trend is the height of the pendulum attachment point along the axis of the tank, referred to as "hinge height" and plotted in Figure 29. The values are measured from a reference point at the top of the tank.

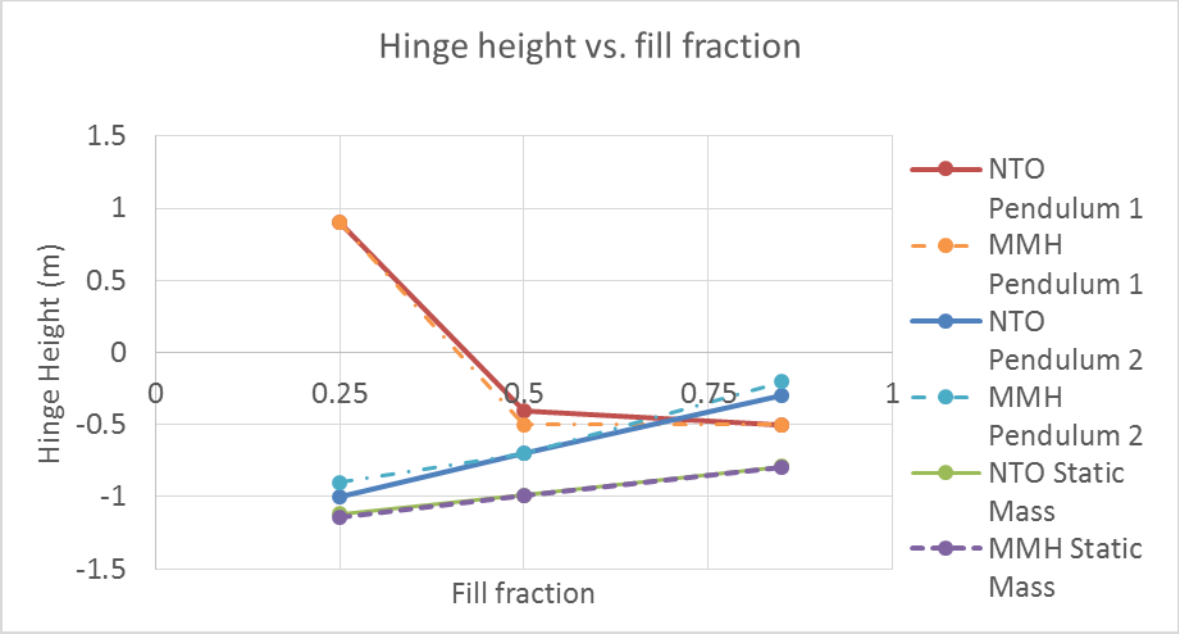

Figure 29. Hinge and static mass height as a function of fill fraction.

The pendulum length was calculated from the frequency and acceleration using the relation $\omega^2 = \frac{g}{L}$. These values were used in conjunction with hinge heights to draw a schematic of the pendulums within the tank, as in Figure 30. From this schematic, the 50% and 85% fill fraction pendulums were all within the region physically occupied by the propellant. In the first iteration of hinge heights, Pendulum 1 for 25% fill was below the tank, so the hinge height was shifted up slightly to keep it within the tank. This shift had minimal impact on the accuracy of modeling moments, since the moments are highly insensitive to changes in hinge height.

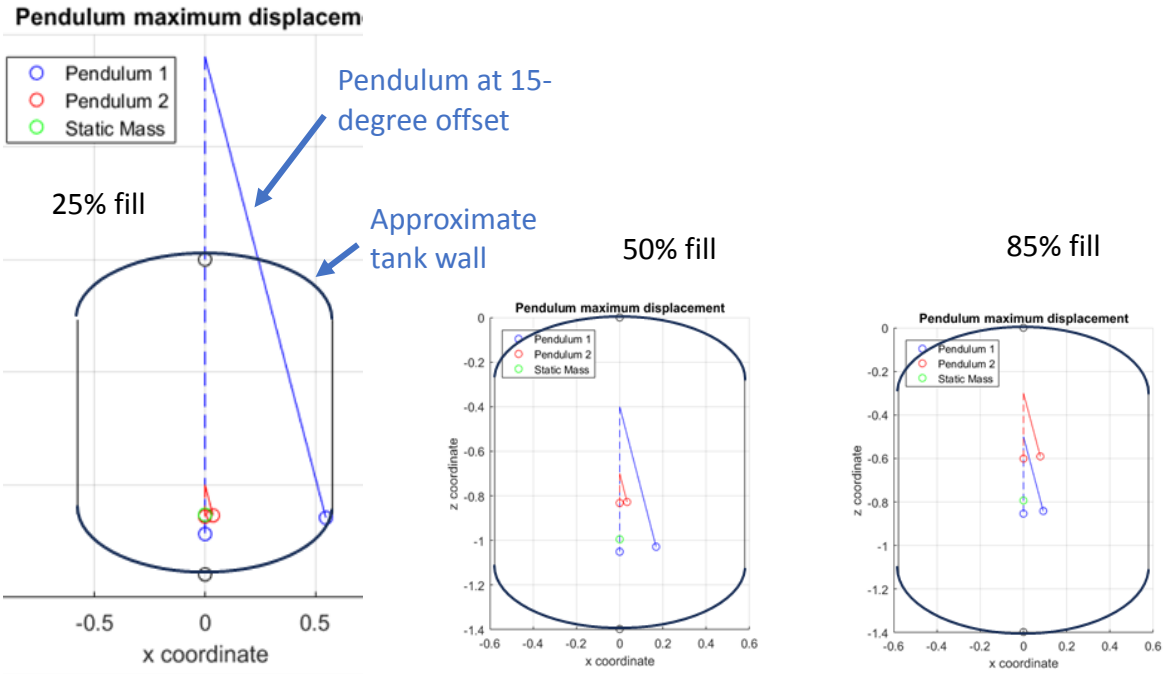

Figure 30. Schematic of pendulums within tank walls.

Discussion of Validity of Assumptions

The analysis in this paper made the following assumptions:

The initial pendulum offset angle is equal to the CFD liquid surface offset angle.

The assumption that the initial pendulum offset angle is equal to the CFD liquid surface offset angle may be incorrect, as will be shown shortly, but there is no other indication of what the initial pendulum offset angle should be. Several test cases were run in which the initial pendulum offset angle was changed to verify if the specific initial pendulum offset angle would give a "best" result. The pendulum parameters did vary for different initial pendulum offset angles, but there was no clear "best" result. To better understand the physics that might allow the pendulum data to match with such a wide variety of pendulum parameters, several more CFD cases were run with different surface initial angle offsets. The results are shown below in Figure 31.

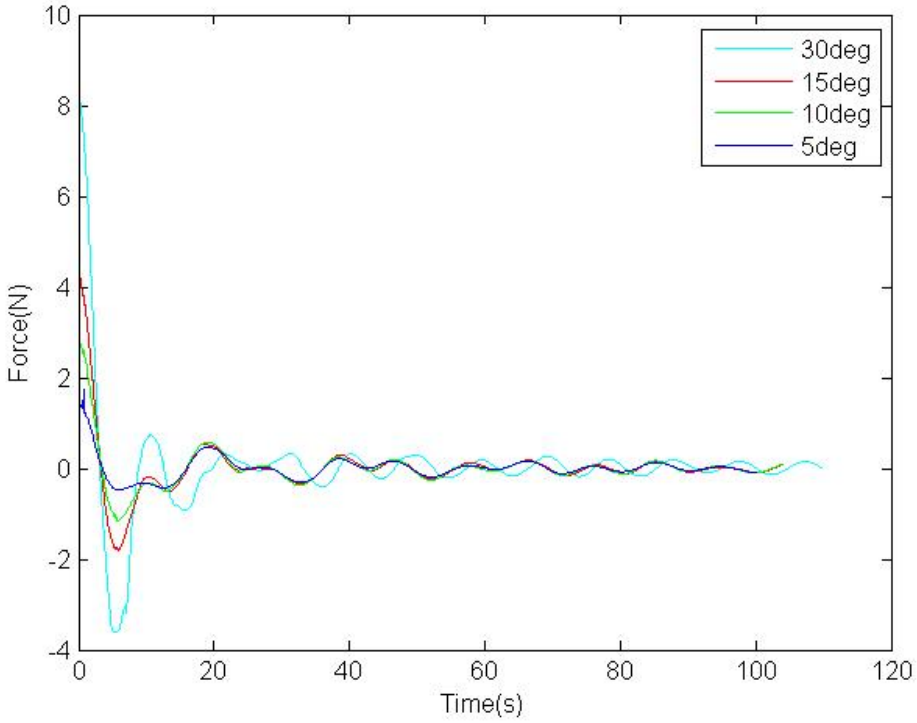

Figure 31. Comparison of CFD forces in the x-direction for different initial surface offset angles.

The CFD results from the 5 deg through 15 deg offset angle cases show that after an initial spike in the force, that the slosh forces become almost identical; however, at an initial offset angle of 30, the behavior is significantly different. It takes several periods before the influence of the initial spike is dampened out for the 30 deg case, with a phase shift as the only remaining difference. Several physical explanations could be put forward, though more research would be needed to prove what is going on. One possible explanation is that the initial sloshing event involves a large percentage of the propellant moving to the bottom of the tank and the majority of this propellant motion is quickly dampened out by the vanes in the PMD. After that, a smaller bulk slosh is left along with sector slosh. The damping of the remaining pendulum slosh is drastically different from the damping in the initial slosh event because less propellant is interacting with the PMD. Additionally, fluid damping is a function of wave height, and the initial condition is a large wave that dampens out much more quickly than the small subsequent waves. As the initial surface offset angle is increased, the influence of the sloshing waves cresting and then rejoining the bulk liquid, as well as the inability of the PMD to fully dampen out the initial bulk movement quickly, leads to non-linearities that cannot be represented by a linear pendulum model. The results from the cases at 25% and 50% fill fraction show this initial spike, but for 80% fill where the PMD is fully immersed, this initial spike does not seem to be present. A large number of CFD slosh cases would need to be run over a range of fill fractions, accelerations, and initial surface offset angles (as well as zero-g initial offsets) to determine how

the initial pendulum angle should be selected. Also, it would be necessary to make the damping non-linear.

With the current data available, choosing the initial angle offset of the pendulum to equal the CFD liquid surface initial angle offset is the most reasonable approach since there is no other physical data within the CFD setup that would indicate another angle.

In light of this, it is critical to realize that using the pendulum model with a smaller initial fluid angle would under-predict the CM and force amplitude in the propellant. This is because the pendulum parameters were derived with an initial propellant and pendulum angle of 15 degrees, and the pendulums' oscillation amplitude is proportional to the initial angle, while the propellant's oscillation amplitude appears to be constant for initial angles between 5-15 degrees. However, for initial disturbance angles greater than 15 degrees, the pendulum model should overpredict the liquid's oscillation amplitude.

The pendulum masses, lengths, damping, and hinge points can be determined by choosing them so that the pendulum results match the CFD results.

The assumption is used because there is not sufficient theory to fix any of these values independent of the CFD results. Because no better theory exists to the author's knowledge, a trial and error method was used. During the trial and error process it was noted that there was not one unique solution. If the mass was increased, the CM oscillation amplitude was higher, but that could be offset by increasing the damping ratio. Because of this, confidence in the accuracy of the mass and damping parameters is lower than the confidence in the accuracy of frequency. Some attempt was made to try and have the initial center of mass offset for the pendulum model equal the initial center of mass offset for the CFD, but this approach did not necessarily improve the matching between the pendulum model and the CFD. If the number of pendulums in the model could vary and the model's damping was non-linear, the approach of matching the initial center of mass offset may be more appropriate.

A two-pendulum model is appropriate for all fill fractions.

In some cases, a three-pendulum model that has the first pendulum dampen out quickly will give good results; in other cases, the behavior resembles a single pendulum model. In the case where a three-pendulum model seems more appropriate, the initial peak in forces is ignored and the two-pendulum model matches the subsequent peaks well. The 25% and 50% fill cases usually fell within this category. If a single pendulum is more appropriate, as was the case with 85% fill, the frequencies were selected such that their constructive and destructive interference contributed to a better match of the CFD CM amplitudes.

The forces and moments caused by the pendulum, as well as the equation describing the pendulum motion, as outlined in the Pendulum Model Derivation section.

The force and moment equations, as well as the equation of motion for the pendulum, were derived from basic principles, using Dodge (2000) as a guide. This equation assumes that mass,

frequency, and damping are constant over time for a given propellant and fill fraction, although the CFD results indicate slight changes over time. The equation also assumes that damping is linear.

The forces which cause the moment on the tank are located at the pendulum and not at the hinge point.

Dodge (2000) suggests that the forces are applied at the pendulum location.

CONCLUSIONS

This paper developed a method for using two-pendulum models to predict slosh behavior on the Europa Clipper mission. The method resulted in a model that can be used to predict slosh behavior to a higher degree of accuracy than a single-pendulum model using less computational power than CFD. The parameters' trends were supported by analytical and experimental literature.

When implementing the pendulum models, it is crucial to recall its limitations. The model can accurately capture slosh behavior either before or after the first peak. High confidence is placed in the predicted pendulum frequencies, while moderate confidence is placed on mass, damping, and hinge locations. The model parameters may reflect inaccuracies in CFD, but experimental data is lacking to verify the CFD results. The pendulum model does not scale well for high fluid disturbance angles, but pendulum parameters based on a low disturbance angle will be conservative when scaled up to higher disturbance angles. The pendulum model assumes damping is constant over time, while it is in fact a function of time and distance traversed by moving fluid. The pendulum model is an approximation of true slosh behavior and these sources of error should be taken into account when designing a system to control slosh.

The methods outlined in this paper could be further validated and refined if experimental data were available in low-gravity slosh experiments.

CONTACT

Wanyi Ng: wanyi.ng@nasa.gov

REFERENCES

Abramson, N. (1966). *The Dynamic Behavior of Liquids in Moving Containers.* Washington, D.C.: U.S. Government Printing Office.

Bauer, H. (1963). Tables and Graphs of Zeros of Cross Product Bessel Functions. *MTP-AERO-63-50 NASA-MSFC.*

Dodge, F. T. (2000). *The New "Dynamic Behavior of Liquids In Moving Containers".* San Antonio, TX: Southwest Research Institute.

Enright, P. J., & Wong, E. C. (1994). Propellant Slosh Models for the Cassini Spacecraft. *AIAA/AAS Astrodynamics Conference.* Scottsdale, AZ: AIAA.

Marsh, W. R., & Knox, B. P. (1970). *USAF Propellant Handbooks Hydrazine Fuels.* Edwards Air Force Base, CA: United States Air Force Systems Command.

Mason, P. &. (2011). The Effects of Propellant Slosh Dynamics on the Solar Dynamics Observatory. *AIAA Guidance, Nagivation, and Control Conference.*

Wright, A. C. (1977). *USAF Propellant Handbooks Nitric Acid/Nitrogen Tetroxide Oxidizers.* Edwards Air Force Base, CA: United States Air Force Systems Command.